




MiR-495-3p and miR-143-3p co-target CDK1 to inhibit the development of cervical cancer

J. Tang¹ · H. Pan² · W. Wang³ · C. Qi³ · C. Gu⁴ · A. Shang^{3,4}  · J. Zhu⁵

Received: 5 February 2021 / Accepted: 26 April 2021 / Published online: 13 August 2021
© Federación de Sociedades Españolas de Oncología (FESEO) 2021

Abstract

Purpose The GEO database and KEGG database-based analyses identified the differential expression of cyclin-dependent kinase 1 (CDK1) in cervical cancer and its involvement in the cell cycle pathway. In the present study, we aim to clarify the role of CDK1 in cervical cancer and the function of upstream microRNA (miR)-143-3p/miR-495-3p.

Methods The expression of miR-143-3p, miR-495-3p, and CDK1 in cervical cancer tissues and cells was determined using RT-qPCR. Cell bioactivities were examined by CCK-8 and flow cytometry. The binding affinity between CDK1 and miR-143-3p/miR-495-3p was investigated using dual luciferase gene reporter assay. A xenograft mouse model of cervical cancer was then established to explore their effect on the tumorigenicity of cervical cancer cells in vivo.

Results CDK1 was found to be the common target gene of miR-143-3p and miR-495-3p. CDK1 overexpression occurred in cervical cancer tissues and cells, while expression of miR-495-3p and miR-143-3p was down-regulated. The viability was inhibited while the apoptosis was promoted in cervical cancer cells in response to miR-143-3p or miR-495-3p overexpression, or CDK1 silencing. Further, miR-143-3p or miR-495-3p overexpression was also substantiated to inhibit the tumorigenicity of cervical cancer cells in vivo, while CDK1 overexpression counteracted their effect.

Conclusion Taken together, miR-143-3p and miR-495-3p co-target CDK1, thereby inhibiting the occurrence and development of cervical cancer.

Keywords miR-143-3p · miR-495-3p · CDK1 · Cervical cancer · Apoptosis · Proliferation

Introduction

Cervical cancer is a frequently occurring gynecological malignancy, presenting high incidence as well as death rates in China [1]. Unfortunately, 569,847 cases were diagnosed with cervical cancer in 2018 on a global scale, and 311,000 deaths were attributed to this disease [2]. It is widely

accepted that persistent infection with carcinogenic human papillomavirus is a leading risk factor for the occurrence of cervical cancer [3]. Cervical cancer is characterized by obviously precancerous lesions together with a long course of cervical intraepithelial neoplasia [4]. The major treatment strategies for cervical cancer include surgery, radiation, and chemotherapy, while the patients also suffer from a relapse rate of 35% as well as a series of side effects [5]. Of note, the roles of microRNAs (miRs) have been highlighted in

Jie Tang, Hongchao Pan and Weiwei Wang are regarded as co-first authors.

✉ A. Shang
shanganquan@sina.com

✉ J. Zhu
hz_zhujichao@yeah.net

¹ Department of Gynecology and Obstetrics, Huzhou Central Hospital, Affiliated Central Hospital of Huzhou Normal University, Huzhou 313003, People's Republic of China

² Department of Laboratory Medicine, Shanghai Simple Gene Medical Laboratory, Shanghai 200025, People's Republic of China

³ Department of Pathology, The Sixth People's Hospital of Yancheng City, Yancheng 224005, People's Republic of China

⁴ Department of Laboratory Medicine, Shanghai Tongji Hospital, Tongji University School of Medicine, Shanghai 200065, People's Republic of China

⁵ Department of Laboratory Medicine, Huzhou Central Hospital, Affiliated Central Hospital of Huzhou Normal University, Huzhou 313003, Zhejiang Province, People's Republic of China

cervical cancer [6]. Herein, the discovery of novel miRs-targeting therapy may be critical for the prevention and treatment of cervical cancer.

miRs are identified as a series of noncoding genes with the regulatory ability on the translation of their target mRNAs [7]. Based on our results of bioinformatics prediction, miR-495-3p and miR-143-3p were very likely to be the upstream regulatory miRs for the important differential gene, cyclin-dependent kinase 1 (CDK1), in cervical cancer. Intriguingly, miR-495-3p has been reported as an important gene for suppression of the carcinogenesis of gastric cancer as well as of that of osteosarcoma [8, 9]. As previously reported, miR-143-3p could enhance the proliferative, migratory, and invasive potentials of C-33A cells in addition to suppressing *in vivo* tumorigenesis in cervical cancer [10]. Moreover, it has been documented that miR-143-3p was downregulated in cervical cancer and participate in the HOTAIR-induced suppression of the viability of cervical cancer cells [11]. CDK1 is regarded as a type of archetypical kinase as well as a crucial regulator that driving cells via G2 phase and mitosis [12]. Intriguingly, upregulated CDK1 by Sp1 was reported to aid in reducing G2/M arrest in cervical cancer cells and enhancing the radioresistance [13]. The downregulation of CDK1 was revealed to aid in the induction of the anti-cancerous effects of CASS in human cervical cancer Hela cells by regulating their proliferation, cytotoxicity, cell cycle, as well as apoptosis [14]. Of note, miR-143 was revealed to regulate CDK2 and CDK4 in hemangioma [15] and miR-495-3p to target CDK6 in colon cancer [16]. With all the above findings taken into consideration, we proposed a hypothesis that miR-143-3p and miR-495-3p may participate in the occurrence and development of cervical cancer by regulating CDK1.

Materials and Methods

Bioinformatics analysis

Through the GEO database (<https://www.ncbi.nlm.nih.gov/geo/>), the cervical cancer expression dataset was retrieved. The “limma” package in R language was utilized for differential analysis, and the “pheatmap” package for delineation of the expression heat map, followed by enrichment analysis utilizing “clusterProfiler” package. A gene–gene interaction analysis was conducted on the selected genes through the STRING database (<https://string-db.org/>), and the position of CDK1 gene in the cell cycle was obtained through the KEGG database (<https://www.kegg.jp/kegg/pathway.html>). The upstream miRs of the CDK1 gene were subsequently predicted through the TargetScan (http://www.targetscan.org/vert_71/), miRDB (<http://mirdb.org/miRDB/>

[index.html](http://www.microrna.org/microrna/home.do?tdsourcetag=s_pcqq_aiomsg)) and microRNAmicro (http://www.microrna.org/microrna/home.do?tdsourcetag=s_pcqq_aiomsg) databases.

Clinical samples

Cervical cancer tissues and adjacent normal tissues were harvested from 60 patients with cervical cancer who underwent cervical surgery performed in Huzhou Central Hospital from July 2016 to January 2018 were enrolled in this study. None of them had received radiotherapy or chemotherapy before surgery. Part of the collected tissues was prepared into paraffin-embedded slides for immunohistochemistry, and the other part was stored in liquid nitrogen for RT-qPCR or Western blot assay.

Cell culture and lentivirus-mediated transduction

HcerEpic (normal cervical epithelial cells) and four cervical cancer cell lines (C4-1 cells, HeLa cells, SiHa cells, and Caski cells) were, respectively, seeded into DMEM medium supplemented with 10% FBS. Next, penicillin and streptomycin (both 100 U/mL) were added to the medium, which was incubated in a CO₂ incubator at 37 °C and 95% humidity.

The cells were seeded in 6-well plates, and the transduction was performed following the protocols of Lipofectamine 2000 (11,668–019, Invitrogen, CA) when cell confluence reached 30–50%. The cells were, respectively, transduced with lentiviral mimic negative control (NC), miR-495-3p mimic, miR-143-3p mimic, short hairpin RNA (shRNA, sh)-NC, sh-CDK1 (lentivirus type 1 or 2 containing sh-CDK1, as labeled as sh-CDK1-1 or sh-CDK1-2), mimic NC + oe-NC, miR-495-3p mimic + oe-NC, miR-143-3p mimic + oe-NC, miR-495-3p mimic + oe-CDK1, miR-143-3p mimic + oe-CDK1. Subsequent experiments were conducted 48 h after lentivirus-mediated transduction. PLKO.1 plasmids inserted with silencing sequences or Fugw-GFP/Plx304 plasmids inserted with cDNA sequences of target genes were combined with auxiliary plasmids (RRE, REV, Vsvg) and packaged by lentivirus (Sangon, Shanghai, China) to construct silencing or overexpression lentivirus. Moreover, the construction of primer sequences and plasmids was completed by Sangon. All the experimental steps were carried out according to the instructions.

CCK-8 assay

Cells were detached, re-suspended, and adjusted to a concentration of 1×10^5 cells/mL before being seeded into 96-well plates (100 μ L/well), followed by incubation overnight. Subsequently, the cells were processed on the basis of the protocols of the CCK-8 kit (Beyotime, Shanghai, China), and the cell viability was examined by measurement of optical density at 450 nm at 24, 48, 72, and 96 h after seeding.

RT-qPCR

The total RNA was extracted from tissues and cells utilizing TRIzol (Invitrogen), the concentration and purity of which were determined using a Nanodrop2000 micro-ultraviolet spectrophotometer (1011U, NanoDrop Technologies, Wilmington). Following the protocols regarding TaqMan MicroRNA Assays Reverse Transcription primer (4,427,975, Applied Biosystems, Carlsbad, CA)/PrimeScript RT reagent Kit (RR047A, Takara, Kyoto, Japan), RNA was reverse-transcribed to cDNA. Primers involved were listed in Supplementary table 1. With the use of ABI7500 qPCR instrument (7500, ABI, Oyster Bay, NY), real-time fluorescent qPCR determination was conducted. U6 was utilized as the internal reference primer for miR, and β -actin as that for CDK1. The relative quantitative ($2^{-\Delta\Delta C_t}$) method was employed for quantification of relative expression.

Dual luciferase reporter gene assay

miR-143-3p mimic and miR-495-3p mimic, and the wide-type (WT) and mutant-type (MUT) CDK1 3'-UTR target site sequences were synthesized. Restriction endonuclease was used for enzyme digestion on the pmir-RB-REPORT™ plasmid, and then synthesized WT and MUT fragments were inserted into the plasmid (both were constructed by Ribobio, Guangzhou, China). The reporter plasmids containing MUT and WT sequence were subsequently co-transferred to HEK293T cells with miR-495-3p mimic or miR-143-3p mimic or mimic NC. After 48 h of transfection, the cells were collected and lysed, and centrifuged to collect the supernatant. Afterwards, the relative luciferase activity (firefly/Renilla) was calculated based on the dual luciferase system (Promega, Madison, WI) and Renilla luciferase detection kit (YDJ2714, Yuduo Biotechnology, Shanghai, China).

Western blot assay

The samples of the cell transfection were lysed with 1 mL of cell lysate for 30 min at 4 °C, and shaken every 10 min. Next, the samples were centrifuged with the lipid layer subsequently discarded. The supernatant, i.e. the protein extract, was subjected to determination of concentration utilizing a BCA kit (20201ES76, Yeasen Biotechnology, Shanghai, China). The lysate was diluted to adjust the loading volume to 30 μ g. After preparation of SDS-PAGE, the samples were mixed with the loading buffer, boiled at 100 °C for 5 min, and then added to each protein lane in an equal amount using a micropipette. Next, the separated protein was transferred to a nitrocellulose membrane, which was then sealed and incubated overnight at 4 °C with primary rabbit anti-mouse antibodies against CDK1 (1, 1000, ab131450, Abcam, Cambridge, UK) and β -actin (1, 5000, ab179467, Abcam) as the

internal control. Horseradish peroxidase (HRP)-labeled goat anti-rabbit against IgG (ab6721, 1, 5000, Abcam) diluent was added to the protein for 1-h incubation at room temperature, followed by color development and fixation. Quantity One software was used to analyze the gray value of each band, with β -Actin as the internal reference.

Flow cytometry

The HeLa and SiHa cells were detached and centrifuged to make a single-cell suspension, which was seeded into 6-well plates (2×10^5 cells/well), followed by incubation under 37 °C and 5% CO₂. Next, the cells were collected, added with 5 μ L of Annexin V-FITC, and then with 5 μ L of propidium iodine (PI), followed by mixing and reaction at room temperature in the dark for 10 min. The cells were examined using a flow cytometer within 1 h.

Cell apoptosis was measured in strict accordance with the Annexin V-FITC/PI apoptosis detection kit (MA0220, Meilun Biotechnology, Dalian, China). The cells were washed with PBS, collected ($2-5 \times 10^5$ cell/mL), and centrifuged (500 g, 5 min) to remove the supernatant. Harvested cells were subsequently re-suspended with 195 μ L binding buffer and incubated with 5 μ L Annexin V-FITC for 10 min in the dark. After that, 10 μ L PI (20 μ g/mL) was added for incubation for 5 min, followed by examination using a flow cytometer.

Xenograft in nude mouse

Twenty-five BALB/c nude mice (4–6 weeks) were randomly assigned into five groups ($n=5$). Lentivirus was used to construct stable-transfected HeLa cells. Briefly, HeLa cells were seeded into 6-well cell plates. When the confluence reached 30–50%, 1 mL of medium was added with 2×10^6 TU corresponding lentivirus and 5 μ g Polybrene, followed by lentivirus-mediated transduction. The transduction was observed under an inverted fluorescence microscope after 2–3 days. Stably transduced cells were obtained, and the medium was replaced with conventional culture medium. The cells were then, respectively, infected with the following lentiviruses: Lv-NC + oe-NC, Lv-miR-495-3p + oe-NC, Lv-miR-143-3p + oe-NC, Lv-miR-495-3p + oe-CDK1, and Lv-miR-143-3p + oe-CDK1. Stably transduced HeLa cells with different treatment were re-suspended and counted (1×10^7 /mL). Next, 100 μ L cell suspension was seeded subcutaneously into the axilla of nude mice. The status of the nude mice and growth of tumors were observed every day after seeding. The short diameter (a) and long diameter (b) of the tumors were recorded every week for the calculation of tumor volume (volume = $a * b^2/2$). After 35 days, the mice were euthanized with CO₂, and the xenografted

tumors were isolated for weighing. Harvested tumor tissues were prepared into paraffin-embedded sections for immunohistochemistry.

Immunohistochemistry

The specimens were treated with 3% methanol H₂O₂ for 20 min, subjected to water bath for antigen retrieval, cooled down, and then incubated with normal goat serum blocking solution (C-0005, Shanghai Haoran Biotechnology, Shanghai, China) for 20 min. After that, the sections were incubated overnight at 4 °C with rabbit anti-human primary antibody against CDK1 (ab131450, 1: 200, Abcam), and then with the goat anti-rabbit secondary antibody against IgG (ab6785, 1: 1000) at 37 °C for 20 min. Subsequently, HRP-labeled streptavidin working solution (0343-10000U, IMUNBIO, Beijing, China) was added for 20-min incubation at 37°C, and DAB (ST033, Whiga, Guangzhou, China) was utilized for color development. Hematoxylin (PT001, Bion Biotechnology, Shanghai, China) was utilized to counterstain the sections for 1 min, which were then immersed in 1% ammonia water to return blue coloration. Next, the sections were processed for microscopic observation and images were photographed. Yellow–brown staining indicated the main expression of CDK1 in the cytoplasm.

Statistical analysis

With the use of SPSS 21.0 (SPSS, IBM, Armonk, NY) statistical software, statistical analysis was performed in this study. Measurement data are expressed as mean ± standard deviation obtained from three independent experiments. Paired *t*-test was used for comparisons between cancer and adjacent normal tissues, and unpaired *t*-test for those between two independent samples. One-way analysis of variance (ANOVA) was used for comparing data between multiples, and repeated measurement or two-way ANOVA with Tukey's post hoc test was performed for comparing data between multiples at different time points. *p* < 0.05 meant that the difference was at a statistically significant level.

Results

CDK1 was up-regulated in cervical cancer tissues and cells

Initially, we performed bioinformatics analysis to screen out differentially expressed genes (DEGs) based on a cervical cancer-related GSE7803 microarray retrieved from the GEO database, which included 10 normal and 31 cervical cancer samples. As a result, 537 DEGs were obtained, and a heat map of the most distinct ones was constructed (Fig. 1a). To

further understand the regulatory functions of these genes in cervical cancer, the KEGG metabolic pathway enrichment analysis was performed on these 537 differential expressions (Fig. 1b). It was found that these differential genes were mainly enriched in the “cell cycle” pathway. The correlation analysis of genes enriched in this metabolic pathway was further carried out, through which a protein–protein interaction network was obtained (Fig. 1c). It was revealed that the CDK1 gene was at the core position in the entire network. In addition, in the KEGG database, a retrieval for the position of CDK1 in the cell cycle pathway (map04110) found that CDK1 was also at the core position in the cell cycle pathway. Further, CDK1 expression in cervical cancer tissue was higher relative to that in adjacent normal tissue (fold change = 2.519; Fig. 1d). The expression of CDK1 in four kinds of cervical cancer cells (C4-1, HeLa, SiHa, Caski) was also significantly increased (Fig. 1e), among which HeLa and SiHa cells showed the highest expression of CDK1 (with fold change of 2.329 and 1.935) and were thus selected for follow-up experiments. These results demonstrated the upregulation of CDK1 in cervical cancer.

Silencing of CDK1 regulated proliferative, apoptotic, migratory, and invasive potentials and cell cycle distribution in cervical cancer cells

Next, we further verified the effect of CDK1 on the biological activities of cervical cancer cells. The efficiency of two kinds of CDK1 silencing sequences in HeLa and SiHa cells was detected. CDK1 expression in response to sh-CDK1-1 or sh-CDK1-2 was significantly decreased, with fold change of 0.129 and 0.326, respectively, relative to that upon sh-NC (Fig. 2a). As the silencing efficiency of sh-CDK1-1 was higher than that of sh-CDK1-2, the sh-CDK1-1 silencing sequence (sh-CDK1) was used for subsequent experiments. Moreover, sh-CDK1 notably diminished the proliferative, migratory, and invasive potentials and increased the number of cells in G0/G1 cell cycle as well as the apoptotic rate (Fig. 2b–f). In summary, the results suggested that CDK1 regulated the proliferative, apoptotic, migratory, and invasive potentials as well as cell cycle distribution of cervical cancer cells.

miR-143-3p and miR-495-3p were downregulated in cervical cancer tissues and cells

To further verify the mechanism of CDK1 upstream gene in cervical cancer, TargetScan, miRDB and microRNA databases were utilized to predict the upstream regulatory miRs of CDK1. The intersection of the predicted results showed that there were two overlapping miRs, namely miR-143-3p and miR-495-3p (Fig. 3a). The expression of miR-143-3p (fold change = 0.318) and miR-495-3p (fold change = 0.384)

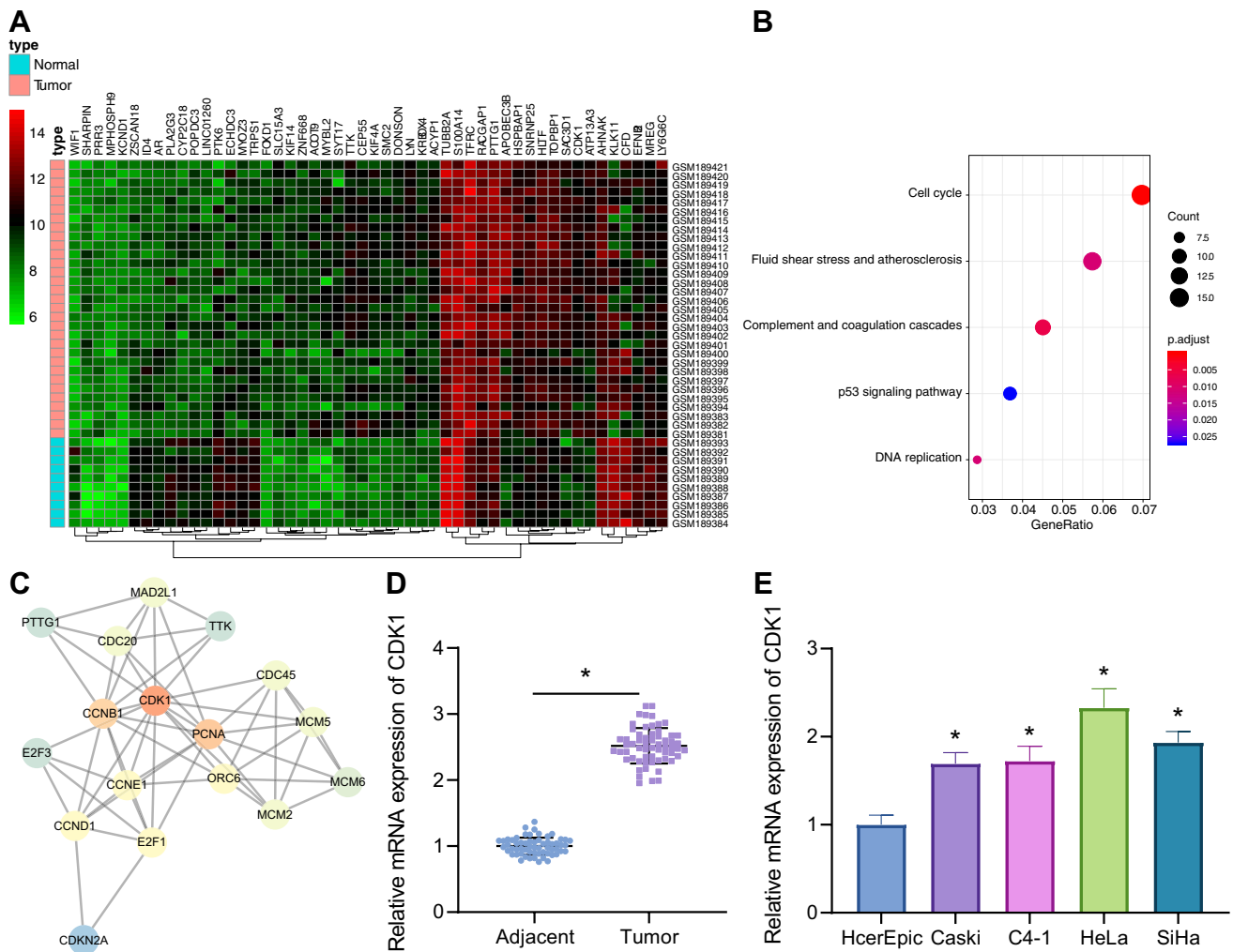


Fig. 1 CDK1 is regulated in cervical cancer tissues and cells. **a** The heatmap for differential gene expression in the cervical cancer microarray. The X-axis represents sample number, and the Y-axis represents gene name. The left dendrogram represents expression clustering, and the upper right histogram is color scale. **b** KEGG pathway enrichment analysis of differential genes. The X-axis represents GeneRatio, and the Y-axis represents KEGG entry name. The right histogram is color scale, and bubble size indicates gene count. **c** The

interaction analysis of enriched genes in cell cycle. Each circle in the network represents a gene, the color of the circle represents the core degree of the gene in the network, and the lines between the circles indicate the interaction between genes. **d** RT-qPCR detection of CDK1 expression in clinical tissues ($n=60$). $*p < 0.05$. vs. adjacent normal tissues. **e**, RT-qPCR was used to detect the expression of CDK1 in cervical cancer cells. $*p < 0.05$. vs. HcerEpic cell line

in cancer tissue was markedly down-regulated, relative to that in adjacent normal tissue (Fig. 3b). Compared with that in HcerEpic cells, the expression of miR-143-3p and miR-495-3p was also notably diminished in C4-1 (fold change: 0.549 for miR-143-3p, 0.438 for miR-495-3p), HeLa (0.126 and 0.167), SiHa (0.211 and 0.267), and Caski (0.412 and 0.375) cells (Fig. 3c). Overall, miR-143-3p and miR-495-3p were down-regulated in cervical cancer.

Overexpression of miR-143-3p or miR-495-3p inhibited the proliferative, migratory, and invasive abilities of cervical cancer cells

Furthermore, the effect of miR-143-3p or miR-495-3p on the malignant phenotypes of cervical cancer cells was investigated. The efficiency of overexpression of miR-143-3p or miR-495-3p in HeLa and SiHa cells was

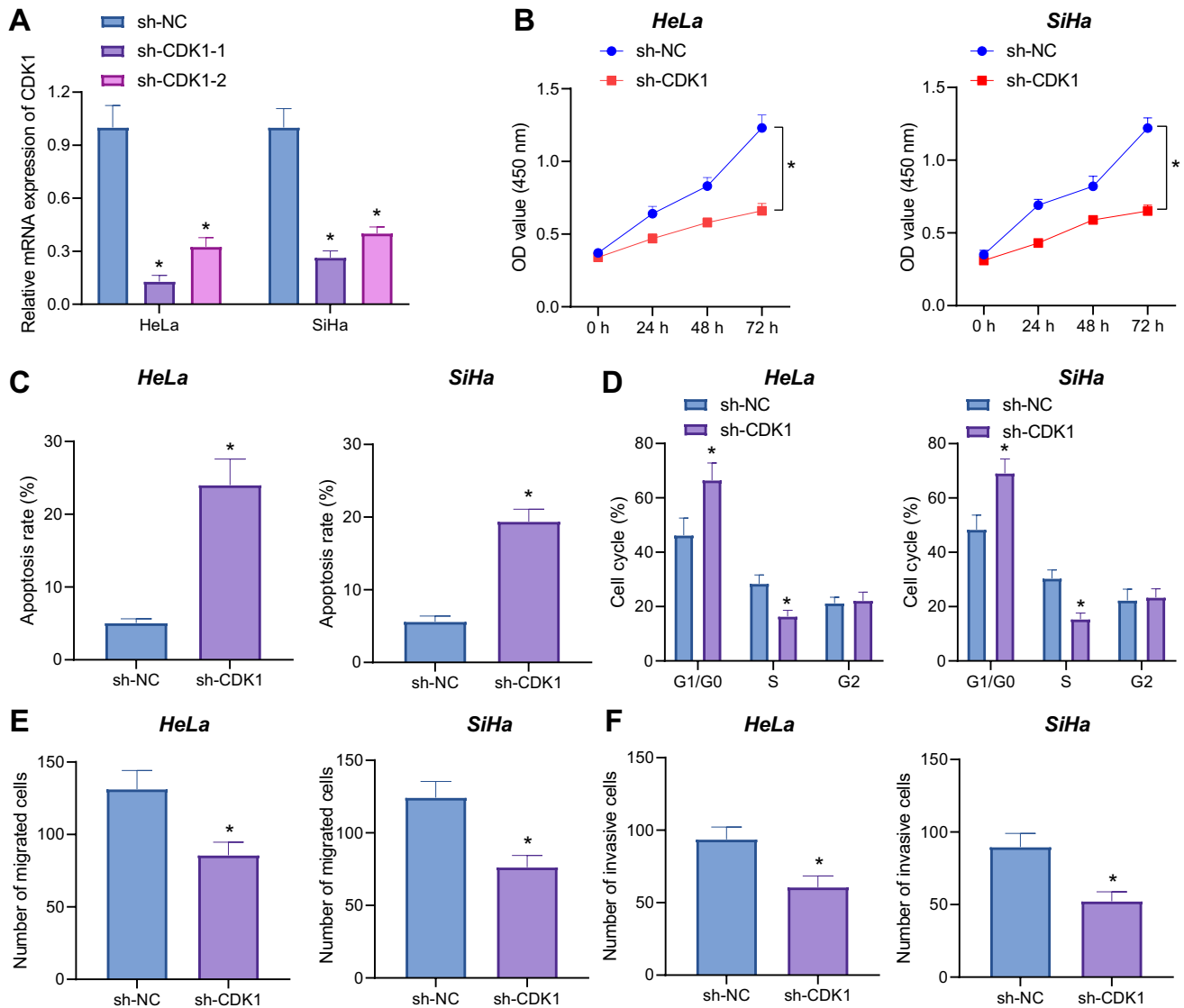


Fig. 2 Silencing of CDK1 regulates viability, apoptosis, cycle, migration, and invasion of cervical cancer cells. A, RT-qPCR was used to detect the efficiency of CDK1 silencing sequence in HeLa and SiHa cells ($*p < 0.05$. vs. sh-NC). B, CCK-8 assay was used to detect the viability of HeLa and SiHa cells ($*p < 0.05$. vs. sh-NC). C, Flow cytometry was used to detect the apoptotic rate of HeLa and SiHa

cells ($*p < 0.05$. vs. sh-NC). D, Flow cytometry was used to detect the changes of cell cycle in HeLa and SiHa cells ($*p < 0.05$. vs. sh-NC). E, Migration of HeLa and SiHa cells as detected by Transwell assay ($*p < 0.05$. vs. sh-NC). F, Invasion of HeLa and SiHa cells as detected by Transwell assay ($*p < 0.05$. vs. sh-NC)

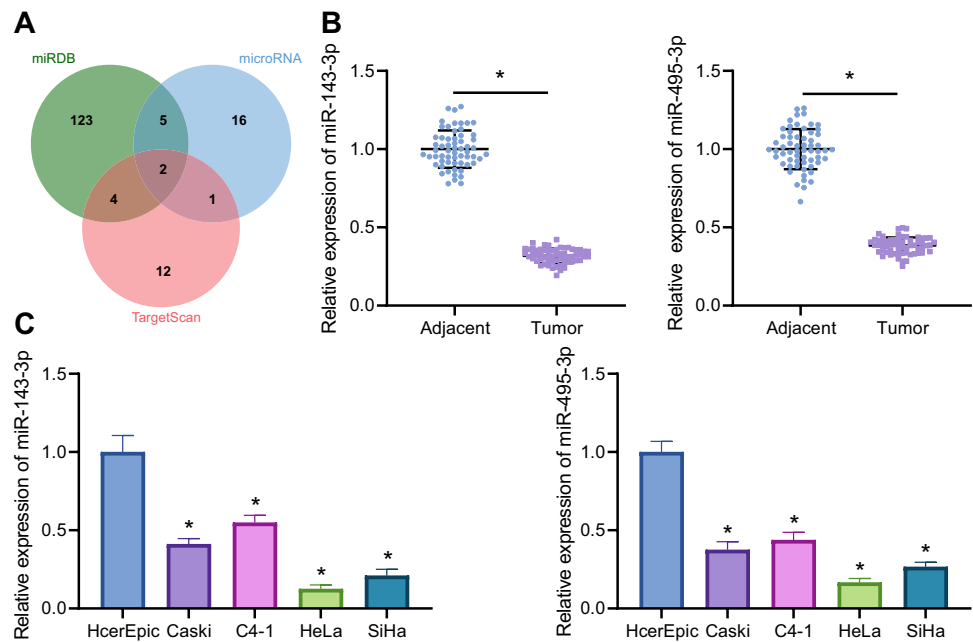
detected. Versus the mimic NC, miR-143-3p mimic led to notably increased expression of miR-143-3p (fold change = 2.184), and miR-495-3p mimic resulted in increased expression of miR-495-3p (fold change = 2.472) (Fig. 4a). Furthermore, miR-143-3p mimic or miR-495-3p mimic decreased the viability of cervical cancer cells, elevated the number of cells in G0/G1 cell cycle as well as the apoptotic rate, and suppressed cell migratory and invasive activities (Fig. 4b–f). Collectively, our results unraveled that miR-143-3p or miR-495-3p was able to modulate the

proliferative, apoptotic, migratory, and invasive potentials as well as cell cycle distribution in cervical cancer cells.

miR-143-3p and miR-495-3p jointly targeted CDK1 to inhibit its expression

We then explored the regulatory function of miR-143-3p/miR-495-3p on CDK1. miR-143-3p and miR-495-3p had binding sites on the 3'UTR of CDK1, respectively (Fig. 5a). In Dual luciferase assay, the luciferase activity decreased in

Fig. 3 miR-143-3p and miR-495-3p are downregulated in cervical cancer tissues and cells. **a** Prediction of upstream regulatory miRs of CDK1. The middle part represents the intersection of three data. **b** Detection of miR-143-3p and miR-495-3p expression in clinical tissues by RT-qPCR ($n=60$). $*p < 0.05$. vs. adjacent normal tissues. **c** Detection of miR-143-3p and miR-495-3p expression in cervical cancer cells by RT-qPCR. $*p < 0.05$. vs. HcerEpic cell line



response to miR-143-3p or miR-495-3p mimic in CDK1-WT whereas no significant change was observed in CDK1-MUT (Fig. 5b). Correlation analysis displayed that in cervical cancer tissue, CDK1 expression was negatively correlated with the expression of miR-143-3p and miR-495-3p (Fig. 5c). Further, CDK1 knockdown did not lead to significant difference in the expression of miR-143-3p and miR-495-3p in HeLa and SiHa cells (Fig. 5d). CDK1 expression upon miR-143-3p mimic (fold change: 0.353 of mRNA expression and 0.293 of protein expression in HeLa cells; 0.254 of mRNA expression and 0.432 of protein expression in SiHa cells) or miR-495-3p mimic (fold change: 0.399 of mRNA expression and 0.349 of protein expression in HeLa cells; 0.335 of mRNA expression and 0.417 of protein expression in SiHa cells) was lower relative to that in response to mimic NC (Fig. 5e, f). Collectively, our data showed that miR-495-3p and miR-143-3p could jointly target and negatively regulate CDK1.

miR-143-3p and miR-495-3p jointly inhibited CDK1 to suppress malignant phenotypes of cervical cancer cells

We further explored whether miR-143-3p and miR-495-3p could attenuate viability and promote apoptosis of cervical cancer cells by modulating CDK1 expression. According to the results, either miR-143-3p mimic or miR-495-3p mimic increased miR-143-3p expression and decreased that of CDK1. Relative to miR-143-3p mimic or miR-495-3p mimic alone, its combination with CDK1 overexpression led to a notable increase in the expression of CDK1 (Fig. 6a). Based on the results, miR-143-3p mimic or miR-495-3p

mimic alone notably reduced the proliferative, migratory, and invasive potentials and increased the cell apoptotic rate and number of cells in G0/G1 phase; whereas its combination with CDK1 overexpression was unraveled to abrogate the aforementioned effects of miR-143-3p mimic or miR-495-3p mimic alone (Fig. 6b–f). Herein, miR-143-3p and miR-495-3p may augment the malignant phenotypes of cervical cancer cells by modulating the expression of CDK1.

miR-143-3p and miR-495-3p attenuated the tumorigenesis ability of cervical cancer cells through targeting CDK1

In order to confirm from in vivo experiments that miR-495-3p and miR-143-3p inhibit the occurrence of cervical cancer through targeted regulation of CDK1, we constructed HeLa cells with overexpression of miR-143-3p or miR-495-3p and those with CDK1 knockdown and then established a xenograft mouse model of cervical cancer. The volume and weight of the tumors in the presence of Lv-miR-495-3p or Lv-miR-143-3p were significantly reduced. Relative to miR-143-3p or Lv-miR-495-3p alone, its combination with CDK1 overexpression contributed to notably increased volume and weight of the tumors (Fig. 7a–c).

RT-qPCR determined the expression of miR-143-3p, miR-495-3p, and CDK1 in tumorigenic tissues, and the results (Fig. 7d) revealed that Lv-miR-495-3p or Lv-miR-143-3p significantly increased the expression of miR-143-3p whereas down-regulated CDK1 expression in the tumors. Versus lentivirus-mediated overexpression of miR-495-3p or miR-143-3p alone, its combination with

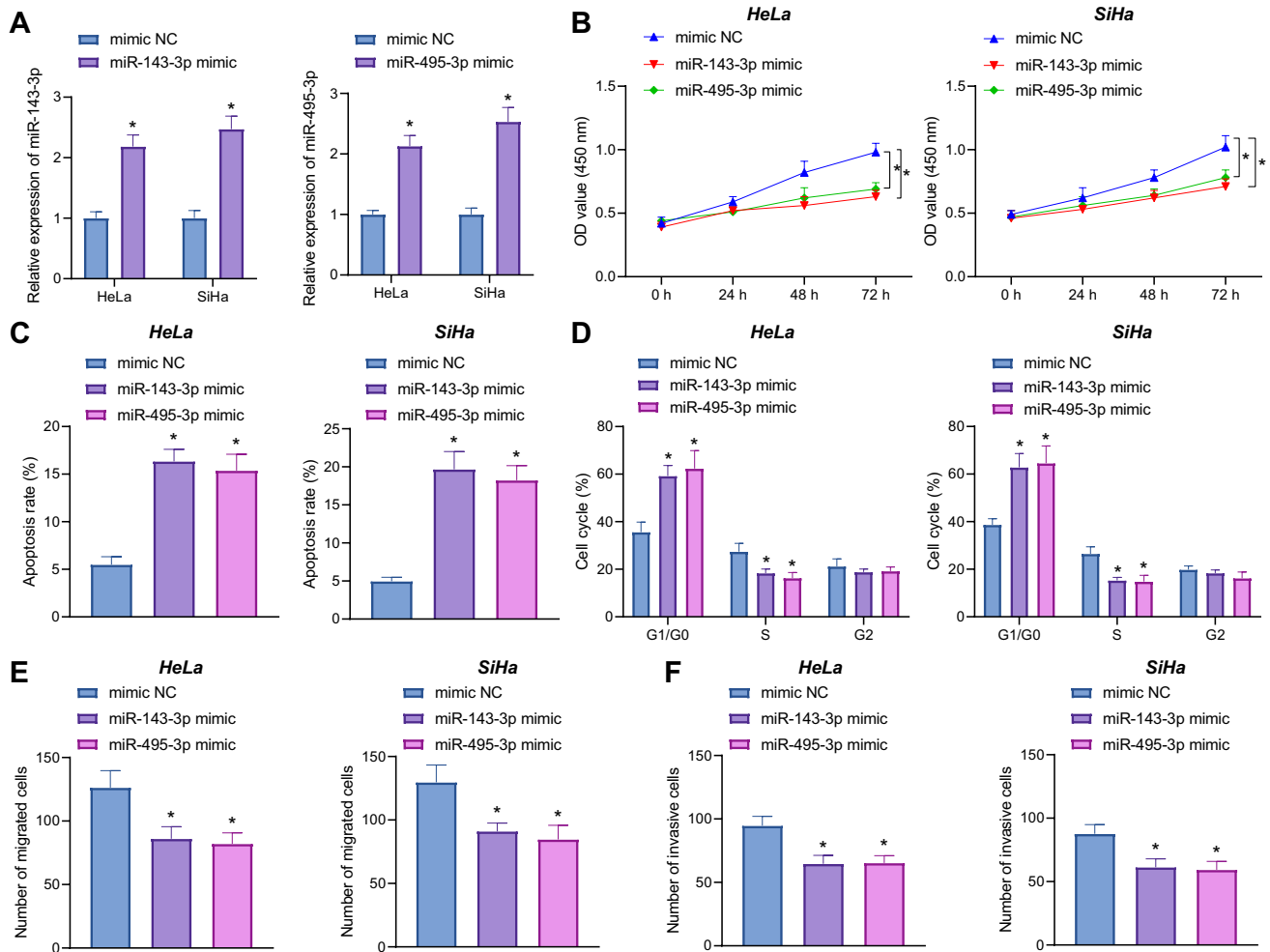


Fig. 4 Overexpression of miR-143-3p or miR-495-3p inhibits viability, apoptosis, cycle, migration, and invasion of cervical cancer cells. **a** RT-qPCR was used to detect the overexpression efficiency of miR-143-3p and miR-495-3p in HeLa and SiHa cells ($*p < 0.05$. vs. mimic NC). **B**, CCK-8 assay was used to detect the viability of HeLa and SiHa cells ($*p < 0.05$. vs. mimic NC). **C**, Flow cytometry was used to

detect the apoptotic rate of HeLa and SiHa cells ($*p < 0.05$. vs. mimic NC). **D**, Cell cycle changes of HeLa and SiHa cells as detected by flow cytometry ($*p < 0.05$. vs. mimic NC). **E**, Migration of HeLa and SiHa cells as detected by Transwell assay ($*p < 0.05$. vs. mimic NC). **F**, Invasion of HeLa and SiHa cells as detected by Transwell assay ($*p < 0.05$. vs. mimic NC)

oe-CDK1 lentivirus led to up-regulated level of CDK1 mRNA expression in the tumors.

Determination of CDK1 expression in tumorigenic tissues by immunohistochemistry showed that, Lv-miR-495-3p + oe-NC or Lv-miR-143-3p + oe-NC contributed to a decrease in the CDK1 positive expression rate in the tumors. In comparison to Lv-miR-495-3p + oe-NC, Lv-miR-495-3p + oe-CDK1 diminished the CDK1 positive expression rate in the tumors. Relative to Lv-miR-143-3p + oe-NC, Lv-miR-143-3p + oe-CDK1 was significantly increased the CDK1 positive expression rate in the tumors (Fig. 7e).

The aforementioned results illuminated that miR-495-3p and miR-143-3p repressed the tumorigenesis of cervical cancer cells through direct regulation of CDK1.

Discussion

In the current study, we defined the role of CDK1 in cervical cancer with the involvement of upstream miR-143-3p/miR-495-3p, and found that miR-143-3p and miR-495-3p exert a suppressive function on the occurrence and development of cervical cancer by co-targeting CDK1.

Of note, we discovered in this study that CDK1 was upregulated in cervical cancer based on the bioinformatics prediction, which was confirmed to display high expression in cervical cancer tissues and cells. We also found that the upstream regulators of CDK1, miR-143-3p, and miR-495-3p were downregulated in cervical cancer. In line with our finding, several prior reports have demonstrated the oncogenic role of CDK1 in cervical cancer. For instance,

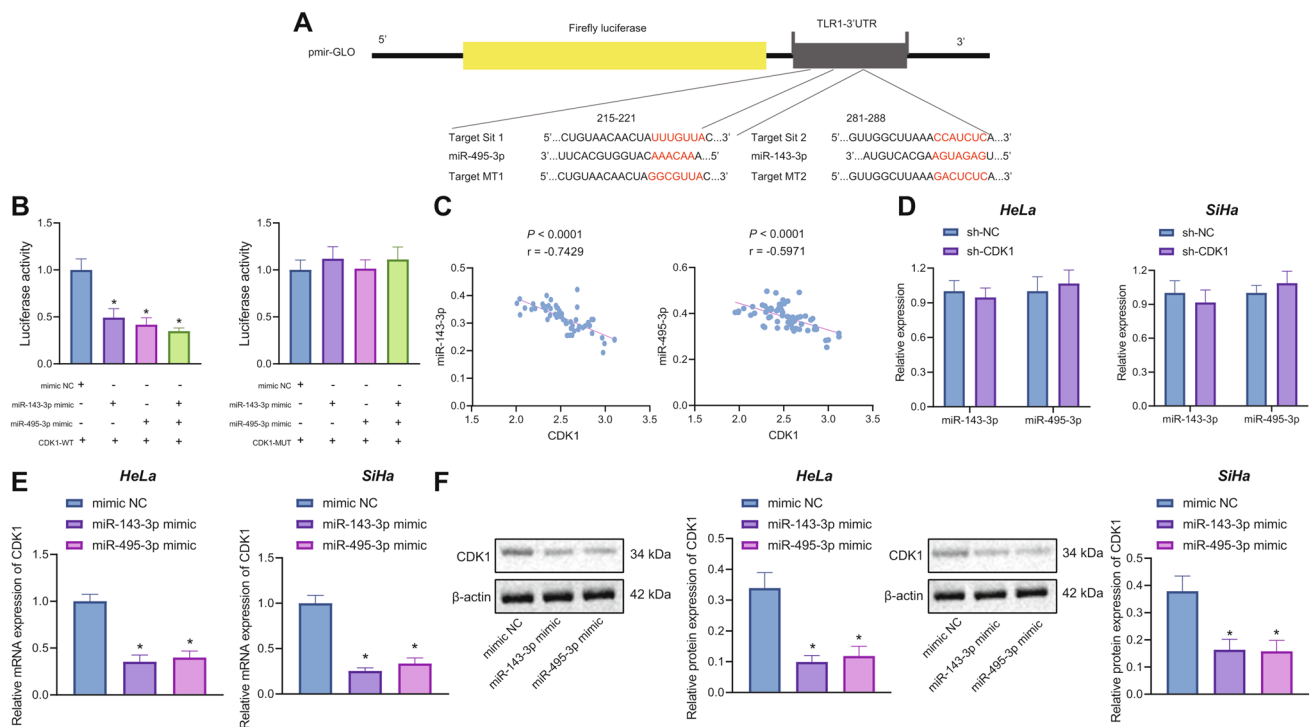


Fig. 5 miR-143-3p and miR-495-3p jointly targets CDK1 to inhibit its expression. **a** Target binding sites between CDK1 and miR-143-3p/miR-495-3p. **b** Dual luciferase reporter gene assay to verify the targeting relationship between miR-495-3p/miR-143-3p and CDK1 ($*p < 0.05$. vs. mimic NC). **c** The correlation between CDK1 and miR-143-3p/miR-495-3p as detected by correlation analysis. **d**

The expression of miR-143-3p and miR-495-3p in HeLa and SiHa cells was detected by RT-qPCR. **e** The mRNA expression of CDK1 in HeLa and SiHa cells was detected by RT-qPCR ($*p < 0.05$. vs. mimic NC). **f** The protein expression of CDK1 in HeLa and SiHa cells after different treatment was detected by Western blot ($*p < 0.05$. vs. mimic NC)

the downregulation of CDK1 was found to aid in the stimulation of the cell apoptosis of cervical cancer [17]. Moreover, CDK1 was revealed to display frequent expression in the processes and pathways involving cell regulation and have a role to confer in the development of cervical cancer [18]. Besides, Chen *et al.* demonstrated that reduced CDK1 expression due to downregulated ROGDI elevated cell accumulation in the G2 phase while repressing cell survival of HeLa and C33A cells [19].

It is noteworthy that miR-143-3p has been suggested to be implicated in the inhibition of cervical cancer. miR-143-3p, interacting with OIP5-AS1, was found to enhance cell viability while suppressing cell apoptosis in cervical cancer [20]. In addition, the use of miR-143-3p inhibitors could promote the viability and invasion of cervical cancer cells and was thus suggested as a potential therapeutic target for cervical cancer [21]. To our knowledge, the function of miR-495-3p in cervical cancer has been rarely reported. In spite of that, several previous studies have revealed the suppressive role of miR-495-3p in other cancers. For instance, Zhao *et al.* demonstrated that miR-495-3p attenuated the proliferative, migratory, and invasive abilities of osteosarcoma cells through targeted regulation of C1q/TNF-related protein 3

[9]. Additionally, downregulated miR-495-3p by lncRNA SNHG20 could enhance the proliferative and invasive potentials of gastric cancer cells [22]. The aforementioned studies could support our finding in regard to the participation of CDK1, miR-143-3p, and miR-495-3p in the pathogenesis of cervical cancer.

Importantly, our finding demonstrated that it was through co-targeting CDK1 that miR-143-3p and miR-495-3p contributed to facilitated occurrence and development of cervical cancer. Notably, an increasing number of studies have reported the regulatory relationship between miR-495-3p, miR-143-3p and CDK members. Intriguingly, miR-495-3p was found to target CDK6 in colon cancer, thereby inhibiting the progression of colon cancer [16]. In addition, it was suggested by Chen *et al.* that miR-495 could lead to downregulated CDK6, thereby suppressing glioblastoma multi-forme cell proliferation [23]. Furthermore, overexpressed miR-143-3p has been highlighted to contribute to downregulation of CDK in airway smooth muscle cells [24]. Besides, it was unveiled that miR-143 could suppress the growth of colon cancer cells in part through the roles of CDK6 [25]. It was also previously reported that miR-143 overexpression could diminish the expression of CDK members including

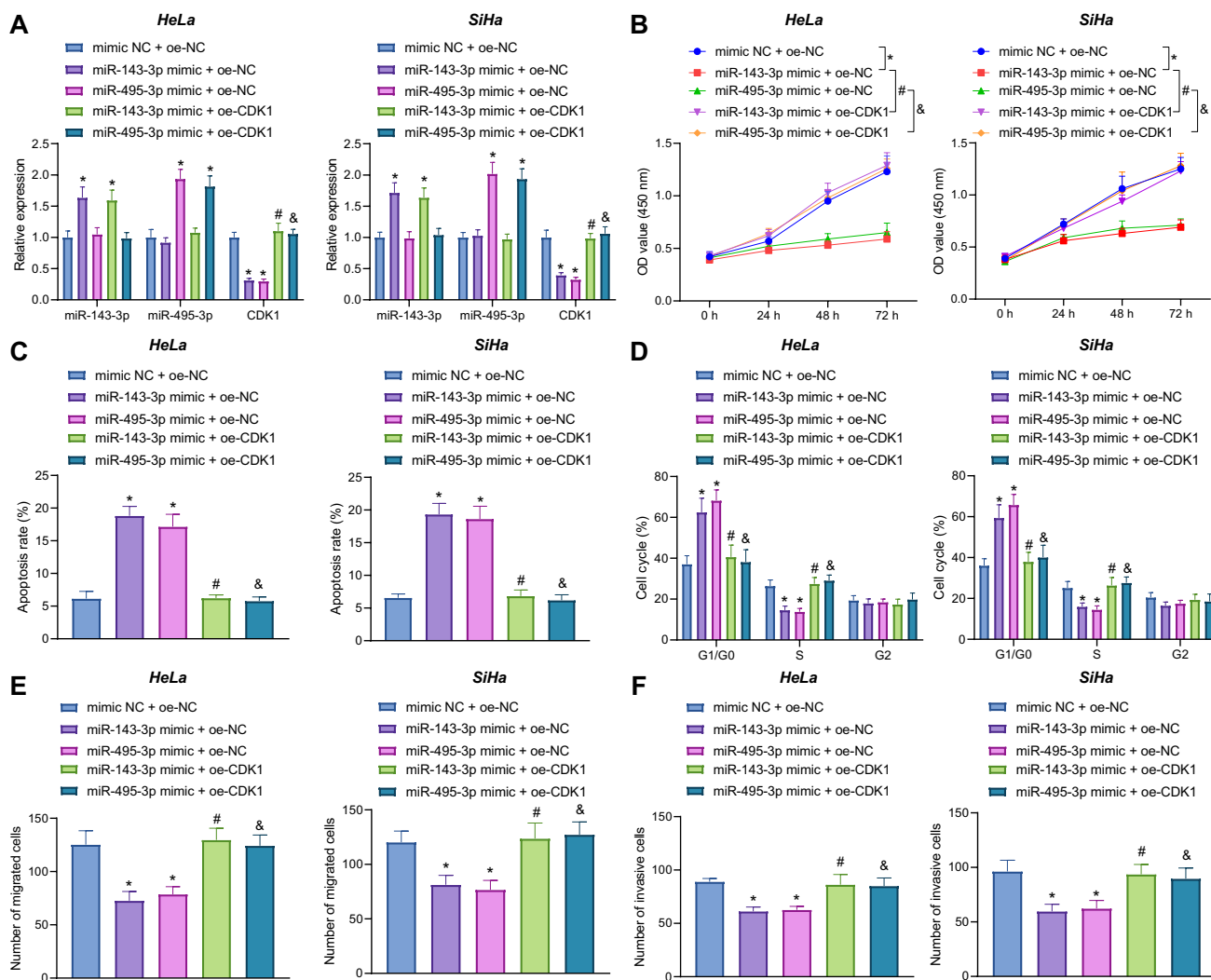


Fig. 6 miR-143-3p and miR-495-3p jointly inhibits CDK1 to suppress malignant phenotypes of cervical cancer cells. **a** The expression of miR-143-3p, miR-495-3p and CDK1 in HeLa and SiHa cells was detected by RT-qPCR ($*p < 0.05$. vs. mimic NC + oe-NC. $\#p < 0.05$. vs. miR-143-3p mimic + oe-NC. & $p < 0.05$. vs. miR-495-3p mimic + oe-NC). **b** The viability of HeLa and SiHa cells was detected by CCK-8 assay ($*p < 0.05$. vs. mimic NC + oe-NC. $\#p < 0.05$. vs. miR-143-3p mimic + oe-NC. & $p < 0.05$. vs. miR-495-3p mimic + oe-NC). **c** The apoptosis of HeLa and SiHa cells was detected by flow cytometry ($*p < 0.05$. vs. mimic NC + oe-NC. $\#p < 0.05$. vs. miR-143-3p mimic + oe-NC. & $p < 0.05$. vs. miR-

495-3p mimic + oe-NC). **d** The cycle of HeLa and SiHa cells was detected by flow cytometry ($*p < 0.05$. vs. mimic NC + oe-NC. $\#p < 0.05$. vs. miR-143-3p mimic + oe-NC. & $p < 0.05$. vs. miR-495-3p mimic + oe-NC). **e**, The migration of HeLa and SiHa cells was detected by Transwell assay ($*p < 0.05$. vs. mimic NC + oe-NC. $\#p < 0.05$. vs. miR-143-3p mimic + oe-NC. & $p < 0.05$. vs. miR-495-3p mimic + oe-NC). **f** The invasion of HeLa and SiHa cells was detected by Transwell assay ($*p < 0.05$. vs. mimic NC + oe-NC. $\#p < 0.05$. vs. miR-143-3p mimic + oe-NC. & $p < 0.05$. vs. miR-495-3p mimic + oe-NC)

CDK2 and CDK4 in hemangioma [15]. In our study, we for the first time discovered the co-targeting mechanism on CDK1 by miR-143-3p and miR-495-3p in cervical cancer. Overall, it was concluded that co-targeting of CDK1 by miR-143-3p in combination with miR-495-3p could regulate the cell biology and in vivo tumorigenesis of cervical cancer.

On the basis of the evidence acquired in the current study, it is substantiated that miR-143-3p and miR-495-3p

co-target CDK1 to suppress the occurrence and development of cervical cancer (Fig. 8). This finding indicates the promising application of miR-143-3p and miR-495-3p in regard of the treatment of cervical cancer. In spite of that, the specific mechanism underlying the modulatory role of CDK1 in cervical cancer warrants further confirmation.

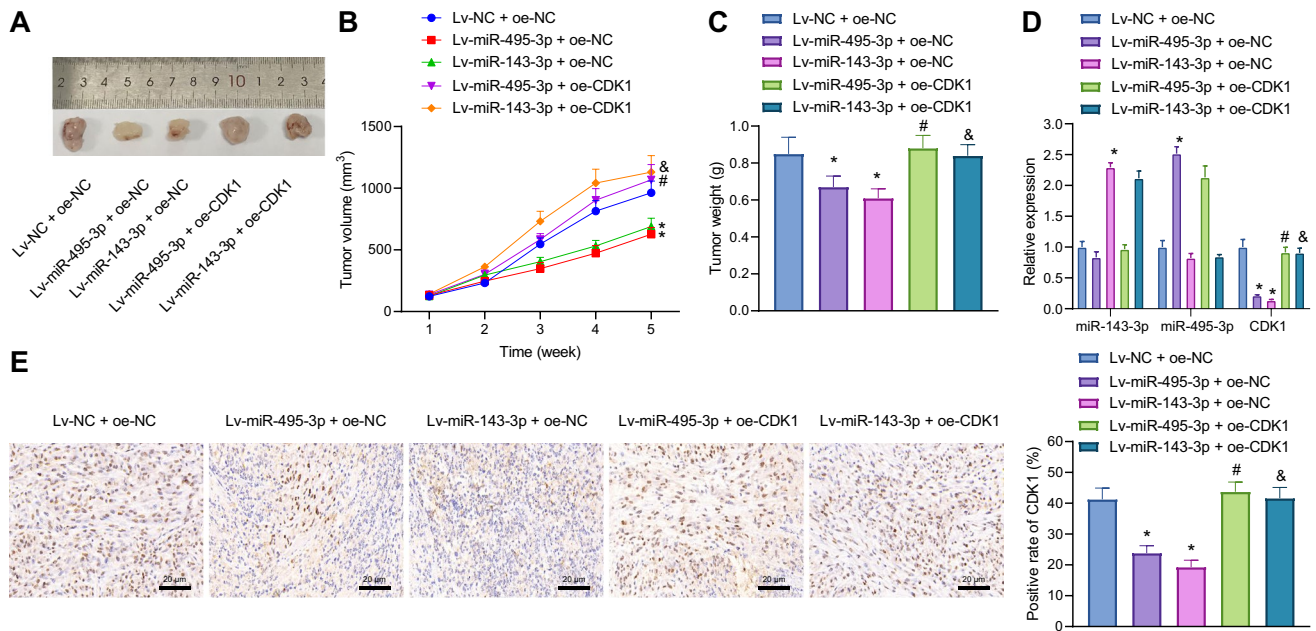
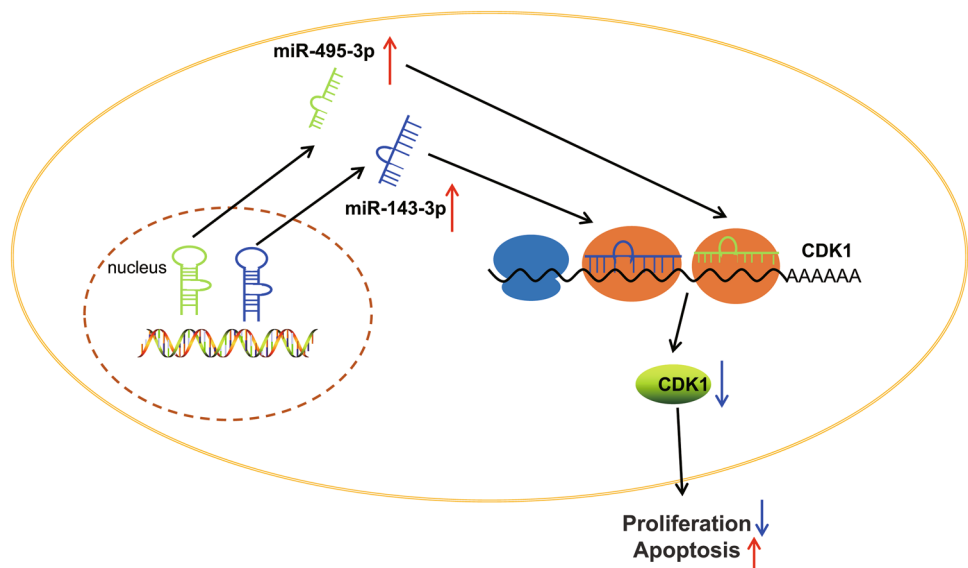


Fig. 7 miR-143-3p and miR-495-3p attenuate the tumorigenesis ability of cervical cancer cells through targeting CDK1. **a** Observation of tumor morphology after different treatment. **b** The statistical plot for tumor volume of nude mice after tumorigenesis. **c** The tumor weight of nude mice after tumorigenesis. **d** The expression of miR-143-3p, miR-495-3p and CDK1 in tumorigenesis tissues as determined by

RT-qPCR. **e** Representative images (left panels) and corresponding quantitative analysis (the right panel) of immunohistochemistry for detection of the expression of CDK1 in tumorigenesis tissues. * $p < 0.05$, vs. Lv-NC + oe-NC. # $p < 0.05$, vs. Lv-miR-495-3p + oe-NC. & $p < 0.05$, vs. Lv-miR-143-3p + oe-NC. $n = 5$

Fig. 8 The mechanism graph of the molecular regulatory network of miR-143-3p and miR-495-3p in cervical cancer. miR-143-3p and miR-495-3p co-target CDK1, thereby suppressing proliferation and promoting apoptosis of cervical cancer cells



Supplementary Information The online version contains supplementary material available at <https://doi.org/10.1007/s12094-021-02687-6>.

Acknowledgements We would like to give our sincere appreciation to the reviewers for their helpful comments on this article.

Author's contribution Jie Tang, Hongchao Pan and Weiwei Wang designed the study. Chunrun Qi and Chenzheng Gu collated the data,

carried out data analyses and produced the initial draft of the manuscript. Jie Tang, Hongchao Pan, Anquan Shang and Jichao Zhu contributed to drafting the manuscript. All authors have read and approved the final submitted manuscript.

Funding None.

Declarations

Conflict of interest The authors have reported that no potential conflicts of interest exist.

Ethical approval This study, under approval of Ethics Committee of Huzhou Central Hospital, was conducted with informed consent provided by all participants, strictly following the *Declaration of Helsinki*. The animal experiments was approved by the Animal Ethics Committee of Huzhou Central Hospital.

Informed consent This study was conducted with informed consent from all participants.

References

- Dai Y, Xie F, Chen Y. Reduced levels of miR-485-5p in HPV-infected cervical cancer promote cell proliferation and enhance invasion ability. *FEBS Open Bio*. 2020;10(7):1348–61. <https://doi.org/10.1002/2211-5463.12869>.
- Diouf D, Diop G, Diarra CAT, Ngom AI, Niane K, Ndiaye M, et al. Systematic screening for cervical cancer in Dakar region: prevalence and correlation with biological and socio-demographic parameters. *Infect Agent Cancer*. 2020. <https://doi.org/10.1186/s13027-020-00290-y>.
- Liu J, Shi Y, Wang L, Wang J, Fan D, Han S, et al. Epidemiology and persistence of cervical human papillomavirus infection among outpatient women in Heilongjiang province: A retrospective cohort study. *J Med Virol*. 2020. <https://doi.org/10.1002/jmv.25899>.
- Li J, Zhou C, Zhou H, Bao T, Gao T, Jiang X, et al. The association between methylated CDKN2A and cervical carcinogenesis, and its diagnostic value in cervical cancer: a meta-analysis. *Ther Clin Risk Manag*. 2016. <https://doi.org/10.2147/TCRM.S108094>.
- Yadav N, Parveen S, Banerjee M. Potential of nano-phytochemicals in cervical cancer therapy. *Clin Chim Acta*. 2020. <https://doi.org/10.1016/j.cca.2020.01.035>.
- Ma D, Zhang YY, Guo YL, Li ZJ, Geng L. Profiling of microRNA-mRNA reveals roles of microRNAs in cervical cancer. *Chin Med J (Engl)*. 2012;125(23):4270–6.
- Williams AE, Moschos SA, Perry MM, Barnes PJ, Lindsay MA. Maternally imprinted microRNAs are differentially expressed during mouse and human lung development. *Dev Dyn*. 2007;236(2):572–80. <https://doi.org/10.1002/dvdy.21047>.
- Eun JW, Kim HS, Shen Q, Yang HD, Kim SY, Yoon JH, et al. MicroRNA-495-3p functions as a tumor suppressor by regulating multiple epigenetic modifiers in gastric carcinogenesis. *J Pathol*. 2018;244(1):107–19. <https://doi.org/10.1002/path.4994>.
- Zhao G, Zhang L, Qian D, Sun Y, Liu W. miR-495-3p inhibits the cell proliferation, invasion and migration of osteosarcoma by targeting C1q/TNF-related protein 3. *Oncol Targets Ther*. 2019. <https://doi.org/10.2147/OTT.S193937>.
- Gang X, Yuan M, Zhang J. Long Non-Coding RNA TMPO-AS1 Promotes cervical cancer cell proliferation, migration, and invasion by regulating miR-143-3p/ZEB1 axis. *Cancer Manag Res*. 2020;12:1587–99. <https://doi.org/10.2147/CMAR.S226409>.
- Liu M, Jia J, Wang X, Liu Y, Wang C, Fan R. Long non-coding RNA HOTAIR promotes cervical cancer progression through regulating BCL2 via targeting miR-143-3p. *Cancer Biol Ther*. 2018;19(5):391–9. <https://doi.org/10.1080/15384047.2018.1423921>.
- Diril MK, Ratnacaram CK, Padmakumar VC, Du T, Wasser M, Coppola V, et al. Cyclin-dependent kinase 1 (Cdk1) is essential for cell division and suppression of DNA re-replication but not for liver regeneration. *Proc Natl Acad Sci USA*. 2012;109(10):3826–31. <https://doi.org/10.1073/pnas.1115201109>.
- Deng YR, Chen XJ, Chen W, Wu LF, Jiang HP, Lin D, et al. Sp1 contributes to radioresistance of cervical cancer through targeting G2/M cell cycle checkpoint CDK1. *Cancer Manag Res*. 2019;11:5835–44. <https://doi.org/10.2147/CMAR.S200907>.
- Li L, Thakur K, Cao YY, Liao BY, Zhang JG, Wei ZJ. Anticarcinogenic potential of polysaccharides sequentially extracted from *Polygonatum cyrtoneuma* Hua in human cervical cancer hela cells. *Int J Biol Macromol*. 2020;148:843–50. <https://doi.org/10.1016/j.ijbiomac.2020.01.223>.
- Huang C, Huang J, Ma P, Yu G. microRNA-143 acts as a suppressor of hemangioma growth by targeting Bcl-2. *Gene*. 2017;628:211–7. <https://doi.org/10.1016/j.gene.2017.07.046>.
- He Z, Dang J, Song A, Cui X, Ma Z, Zhang Z. NEAT1 promotes colon cancer progression through sponging miR-495-3p and activating CDK6 in vitro and in vivo. *J Cell Physiol*. 2019;234(11):19582–91. <https://doi.org/10.1002/jcp.28557>.
- Han B, Zhang Y, Zhang Y, Bai Y, Chen X, Huang R, et al. Novel insight into circular RNA HECTD1 in astrocyte activation via autophagy by targeting MIR142-TIPARP: implications for cerebral ischemic stroke. *Autophagy*. 2018;14(7):1164–84. <https://doi.org/10.1080/15548627.2018.1458173>.
- Luo Y, Wu Y, Peng Y, Liu X, Bie J, Li S. Systematic analysis to identify a key role of CDK1 in mediating gene interaction networks in cervical cancer development. *Ir J Med Sci*. 2016;185(1):231–9. <https://doi.org/10.1007/s11845-015-1283-8>.
- Chen YF, Cho JJ, Huang TH, Tseng CN, Huang EY, Cho CL. Downregulation of a novel human gene, ROGD1, increases radiosensitivity in cervical cancer cells. *Cancer Biol Ther*. 2016;17(10):1070–8. <https://doi.org/10.1080/15384047.2016.1219818>.
- Song L, Wang L, Pan X, Yang C. lncRNA OIP5-AS1 targets ROCK1 to promote cell proliferation and inhibit cell apoptosis through a mechanism involving miR-143-3p in cervical cancer. *Braz J Med Biol Res*. 2020;53(1):e8883. <https://doi.org/10.1590/1414-431X20198883>.
- Yang J, Jiang B, Hai J, Duan S, Dong X, Chen C. Long noncoding RNA opa-interacting protein 5 antisense transcript 1 promotes proliferation and invasion through elevating integrin alpha6 expression by sponging miR-143-3p in cervical cancer. *J Cell Biochem*. 2019;120(1):907–16. <https://doi.org/10.1002/jcb.27454>.
- Cui N, Liu J, Xia H, Xu D. lncRNA SNHG20 contributes to cell proliferation and invasion by upregulating ZFX expression sponging miR-495-3p in gastric cancer. *J Cell Biochem*. 2019;120(3):3114–23. <https://doi.org/10.1002/jcb.27539>.
- Chen SM, Chen HC, Chen SJ, Huang CY, Chen PY, Wu TW, et al. MicroRNA-495 inhibits proliferation of glioblastoma multiforme cells by downregulating cyclin-dependent kinase 6. *World J Surg Oncol*. 2013;11:87. <https://doi.org/10.1186/1477-7819-11-87>.
- Cheng W, Yan K, Xie LY, Chen F, Yu HC, Huang YX, et al. MiR-143-3p controls TGF-beta1-induced cell proliferation and extracellular matrix production in airway smooth muscle via negative regulation of the nuclear factor of activated T cells 1. *Mol Immunol*. 2016;78:133–9. <https://doi.org/10.1016/j.molimm.2016.09.004>.
- Zhu H DU, Mustafi R, et al. 679 Putative Tumor Suppressors miR-143 and miR-145 Inhibit HCT116 Colon Cancer Cell Growth in Tumor Xenografts, Roles of K-RAS, MYC, Ccnd2 and Cdk6. *Gastroenterology*. 2010;138(5-suppl-S1):S–93.

Publisher's Note Springer Nature remains neutral with regard to jurisdictional claims in published maps and institutional affiliations.